

Updated analysis of jet quenching at RHIC and LHC within the light cone path integral approach

B.G. Zakharov

L.D. Landau Institute for Theoretical Physics, GSP-1, 117940,
Kosygina Str. 2, 117334 Moscow, Russia

E-mail: bgz@itp.ac.ru

Abstract. We present results of a detailed analysis of experimental data on the nuclear modification factor R_{AA} and the flow coefficient v_2 for light hadrons from RHIC for 0.2 TeV Au+Au collisions and from LHC for 2.76 and 5.02 TeV Pb+Pb, and 5.44 TeV Xe+Xe collisions. We perform calculations within the light-cone path integral approach to induced gluon emission. We use running α_s which is frozen at low momenta at some value α_s^{fr} . We find that the RHIC data support somewhat larger value of α_s^{fr} . For the χ^2 optimized values of α_s^{fr} , the theoretical predictions are in reasonable agreement with data on R_{AA} and v_2 . Calculations made for different formation times and life-times of the QGP show that jet quenching at the RHIC and LHC energies is only weakly sensitive to the initial and final stages of the QCD matter evolution.

1. Introduction

It is widely believed that strong suppression of the high- p_T particle spectra in AA collisions (usually called the jet quenching) observed first at RHIC, and later at the LHC, is due to parton energy loss in the quark-gluon plasma (QGP) produced in the initial stage of nucleus collisions (for reviews on the jet quenching phenomenon, see, e.g., [1, 2]). For the RHIC and LHC conditions, the dominating contribution to the parton energy loss comes from the induced gluon radiation caused by parton multiple scattering in the QGP [3, 4, 5, 6, 7, 8, 9], and the effect of the collisional energy loss [10] turns out to be relatively weak [11, 12, 13]. In the pQCD picture, for the QGP modeled by a system of the Debye screened color centers [3], the induced gluon spectrum can be expressed via the Green function of a 2D Schrödinger equation with an imaginary potential [6, 4], in which the longitudinal coordinate z plays the role of time. This potential is $\propto n\sigma_{q\bar{q}}(\rho)$, where n is the QGP number density and $\sigma_{q\bar{q}}(\rho)$ is the dipole cross section for scattering of a color singlet $q\bar{q}$ pair off the QGP constituent (here, ρ is the size of the $q\bar{q}$ -pair). For the quadratic approximation $\sigma_{q\bar{q}}(\rho) \approx C\rho^2$, the Hamiltonian of the Schrödinger equation takes the harmonic oscillator (HO) form with a complex frequency $\Omega^2 \propto \hat{q}$ with $\hat{q} = 2Cn$. At the same time, the quantity \hat{q} , commonly called

the transport coefficient, characterizes the L -dependences of the parton p_T -broadening in the medium: $\langle p_T^2 \rangle = L\hat{q}$ [5].

In the HO approximation the induced gluon spectrum for massless partons in a uniform medium can be evaluated analytically [4, 14]. In [15] it was shown that, for the Bjorken like QGP expansion [16], the total radiative energy loss in the HO approximation can be expressed via that for a static medium with an equivalent linear averaged transport coefficient: $\hat{q}_{st} = \frac{2}{L^2} \int d\tau \tau \hat{q}(\tau)$. By numerical calculations it was found [17] that such a dynamical scaling, to rather good accuracy, holds also for the gluon spectrum. Making use of this dynamical scaling law simplifies greatly jet quenching calculations for an expanding QGP [18]. However, in a recent analysis [19] it was demonstrated that the approximation of the dynamical scaling may be too crude for precise modeling of the jet quenching phenomenon. In any case, the HO approximation itself cannot be regarded as satisfactory for accurate jet quenching simulations. The apparent shortcoming of the HO approximation is that the opacity expansion series of the gluon spectrum for massless partons does not contain the $N = 1$ (and all odd terms) rescattering contribution [20] (see also [21]). The $N = 2k + 1$ rescattering terms become nonzero due to the Coulomb effects, that lead to logarithmic dependence of the factor $C = \sigma_{q\bar{q}}(\rho)/\rho^2$ at $\rho \rightarrow 0$, and mass effects [20, 22]. These effects may change drastically the HO gluon spectrum in the regime when gluon formation length becomes comparable or larger than the parton path length in the QGP [20, 22].

The absence of the leading $N = 1$ term in the HO approximation is not very important in the limit of strong Landau-Pomeranchuk-Migdal (LPM) suppression, when the typical number of rescatterings becomes very large. However, for the QGP produced in AA -collisions we have a situation when the contribution of the $N = 1$ term dominates the radiative parton energy loss [8]. This fact stimulated the jet quenching analyses (see, e.g., [23, 24] and references therein) based on the GLV formalism [8] with accounting for only $N = 1$ term. In the models restricted to the $N = 1$ rescattering, the effect of higher order rescatterings can be partly absorbed into a redefinition of α_s (or some of the QGP parameters). But this should influence the predictions for quantities that depend on variation of the LPM suppression (because the magnitude of the LPM effect varies significantly with the parton energy, the QGP size and density). As a result, such important jet quenching characteristics as the p_T - and centrality-dependence of the R_{AA} , azimuthal flow coefficient v_2 may have considerable theoretical uncertainties.

In this work we continue our investigations [25, 26, 27, 28] of the jet quenching within the light-cone path integral (LCPI) approach [6] to the induced gluon emission. The main motivation of the present work is to perform a more comprehensive analysis of the data from RHIC and LHC including the recent LHC data for 5.02 TeV Pb+Pb and 5.44 TeV Xe+Xe collisions. The LCPI formalism [6] is free from the above mentioned problems inherent to the models based on the HO and $N = 1$ approximations. It allows one to perform calculations for an arbitrary number of rescatterings beyond the HO approximation for massive partons with accurate treatment of the finite-size effects. Also, it is free from the restriction to the strong LPM suppression (which is needed in the

BDMPs formulation [4]). The LCPI formalism [6] is applicable to any induced process of the type $a \rightarrow bc$ both in QED and QCD. It is based on the path integral representation in the coordinate space for the in-medium wave functions of fast particle on the light-cone $t - z = \text{const}$. For the case of a uniform, infinite medium the LCPI formulation is equivalent [29] to the the AMY [9] approach, formulated in the momentum space. The induced gluon/photon spectrum was originally written in [6] in terms of Green's function of the Schrödinger equation. Since the Green function is singular at $z \rightarrow 0$, the Green function representation is inconvenient for numerical calculations beyond the HO approximation. In [30], by solving the Schrödinger equation backward in time/ z , we obtained a representation of the induced gluon spectrum for a finite-size medium in terms of a solution to the Schrödinger equation with a smooth boundary condition, which is convenient for numerical computations (this form has been rediscovered later in [31]).

Unfortunately, numerical solving the Schrödinger equation requests a rather large computational time. This renders difficult numerical jet quenching simulations for realistic scenarios of the QGP formation and evolution. This forces to use simplified models for the initial QGP fireball and its hydrodynamic evolution, in which the computational cost may be reduced. In [25] we have performed calculations of the nuclear modification factor R_{AA} within the LCPI scheme [30] with realistic dipole cross section using the model of the QGP fireball with a uniform density distribution in the transverse plane and with the Bjorken 1+1D hydrodynamical longitudinal expansion. For this model the density profile along the fast parton trajectory for each jet production point turns out to be the same (only its length L varies). This makes it possible to perform first tabulating the L -dependence of the induced gluon spectrum and then to use interpolation in computation of the medium modified jet fragmentation functions (FFs) for arbitrary positions of the jet production. This procedure greatly reduces the computational time. In [26, 27, 28] we used the model [25] for analysis of the RHIC and LHC data on the nuclear modification factor R_{AA} in 0.2 TeV Au+Au collisions at RHIC and 2.76 TeV Pb+Pb collisions at the LHC. It was found that predictions of the LCPI approach are in reasonable agreement with data. But this is only possible if one uses somewhat larger α_s for RHIC.

In the present work, as in [26, 27, 28] we use the method of [30] for calculations of the induced gluon spectrum with realistic dipole cross section. We use a somewhat improved version of the scheme of [25] for evaluating the medium modified FFs from the one gluon spectrum (see appendix B for details). We perform comparison with data on both the nuclear modification factor R_{AA} and the azimuthal anisotropy v_2 for different centralities. Contrary to our previous jet quenching analyses [26, 27, 28], where a visual comparison with data was performed, in the present study we perform an accurate χ^2 fit to the data. Our results for the nuclear modification factor R_{AA} agree quite well with experimental data. Although we do not include the data on v_2 in the χ^2 analysis, our predictions for v_2 are in reasonable agreement with the data as well. However, similarly to our previous analyses, we find that the description of the RHIC

data requires somewhat bigger α_s than that for the LHC. In the present study it is demonstrated with the help of an accurate χ^2 analysis.

The paper is organized as follows. In Section 2, we briefly review the basic aspects of our jet quenching model. In Section 3, we perform the χ^2 fit of the experimental data on R_{AA} for finding the optimal α_s , and then confront the theoretical results with data on R_{AA} and v_2 . Conclusions are contained in Section 4. Some of the details of our calculations are given in two appendices. In appendix A, we give the basic formulas for evaluation of the induced gluon spectrum. The method for calculation of the in-medium FFs is considered in appendix B.

2. Theoretical framework

In this section we outline the main aspects of our method for calculating the nuclear modification factor R_{AA} and the azimuthal anisotropy v_2 . It is similar to the method used in our previous jet quenching analyses [25, 26, 28], to which the interested reader is referred for details.

2.1. Nuclear modification factor

We will consider the central rapidity region around $y = 0$. We write the nuclear modification factor R_{AA} for given impact parameter b of AA -collision, the hadron transverse momentum \mathbf{p}_T and rapidity y as

$$R_{AA}(b, \mathbf{p}_T, y) = \frac{dN(A + A \rightarrow h + X)/d\mathbf{p}_T dy}{T_{AA}(b) d\sigma(N + N \rightarrow h + X)/d\mathbf{p}_T dy}, \quad (1)$$

where $T_{AA}(b) = \int d\boldsymbol{\rho} T_A(\boldsymbol{\rho}) T_A(\boldsymbol{\rho} - \mathbf{b})$, $T_A(\boldsymbol{\rho}) = \int dz \rho_A(\sqrt{\rho^2 + z^2})$ is the nuclear thickness function (with ρ_A the nuclear density). The nominator of (1) is the differential yield of the process $A + A \rightarrow h + X$ (for clarity we omit the arguments b and \mathbf{p}_T). It can be written in terms of the medium-modified hard cross section $d\sigma_m/d\mathbf{p}_T dy$ as

$$\frac{dN(A + A \rightarrow h + X)}{d\mathbf{p}_T dy} = \int d\boldsymbol{\rho} T_A(\boldsymbol{\rho} + \mathbf{b}/2) T_A(\boldsymbol{\rho} - \mathbf{b}/2) \frac{d\sigma_m(N + N \rightarrow h + X)}{d\mathbf{p}_T dy}. \quad (2)$$

We write $d\sigma_m/d\mathbf{p}_T dy$ in the form

$$\frac{d\sigma_m(N + N \rightarrow h + X)}{d\mathbf{p}_T dy} = \sum_i \int_0^1 \frac{dz}{z^2} D_{h/i}^m(z, Q) \frac{d\sigma(N + N \rightarrow i + X)}{d\mathbf{p}_T^i dy}, \quad (3)$$

where $\mathbf{p}_T^i = \mathbf{p}_T/z$ is the transverse momentum of the initial hard parton, $d\sigma(N + N \rightarrow i + X)/d\mathbf{p}_T^i dy$ is the ordinary hard cross section, $D_{h/i}^m(z, Q)$ is the medium-modified FF for transition of a parton i with the virtuality $Q \sim p_T^i$ to the final particle h . The FF $D_{h/i}^m$ depends on the medium parameters along the jet path in the medium:

$$\boldsymbol{\rho}(\tau) = \boldsymbol{\rho}_j + \mathbf{v}\tau, \quad (4)$$

where $\boldsymbol{\rho}_j$ is transverse coordinate of the hard process, and $\mathbf{v} \approx \mathbf{p}_T/|\mathbf{p}_T|$ is the jet velocity. Since $|\mathbf{v}| \approx 1$, the proper time τ in (4) coincides with the jet path length. The

variation of the medium profile with the jet azimuthal angle generates the dependence of the nuclear modification factor on the direction of the hadron momentum relative to the reaction plane. We consider the event-averaged smooth evolution of the QGP fireball. In this approximation, the azimuthal dependence can be characterized by the even azimuthal coefficients v_{2n} , which, for a given impact parameter can be written as

$$v_{2n}(p_{\perp}) = \frac{1}{2\pi R_{AA}(b, p_{\perp})} \int d\phi R_{AA}(b, \mathbf{p}_T, y) \cos(2n\phi), \quad (5)$$

where

$$R_{AA}(b, p_{\perp}) = \frac{1}{2\pi} \int d\phi R_{AA}(b, \mathbf{p}_T, y) \quad (6)$$

is the azimuthally averaged nuclear modification factor. For comparison with experimental quantities measured in a centrality bin $\Delta(c_1, c_2)$, in the above formulas one should perform integration over the impact parameter region (b_1, b_2) with $b_{1,2}$ written in terms of the $c_{1,2}$ (the b -integrations should be performed separately for the numerators and denominators). Experimentally, the centrality of an event is defined in terms of the soft charged particle multiplicity (in some kinematic region). To a very good accuracy (except for the most peripheral collisions) the relation between the centrality and the impact parameter reads $c = \pi b^2 / \sigma_{in}^{AA}$ [32].

As usual, we assume that the final particles are formed outside the medium. We also assume that for medium-modified parton-to-parton FFs, the DGLAP stage precedes the induced gluon emission stage. With the help of the formation length arguments, one can show that this approximation should be reasonable at least for jets with energy $\lesssim 100$ GeV [25]. In this approximation, $D_{h/i}^m$ symbolically can be written as

$$D_{h/i}^m(Q) \approx D_{h/j}(Q_0) \otimes D_{j/k}^{in} \otimes D_{k/i}(Q), \quad (7)$$

where \otimes denotes z -convolution, $D_{k/i}$ is the DGLAP parton FF for $i \rightarrow k$ transition, $D_{j/k}^{in}$ is the in-medium FF for $j \rightarrow k$ transition due to induced gluon emission, and $D_{h/j}$ is the vacuum FF for transition of the parton j to the final particle h .

For the vacuum FFs $D_{h/j}(z, Q_0)$ we use the KKP [33] parametrization with $Q_0 = 2$ GeV. In numerical calculations we compute the DGLAP FFs $D_{k/i}$ by interpolating from a 2D (z, Q) grid, created with the help of the PYTHIA event generator [34]. The FFs for pp collisions needed to calculate R_{AA} have been obtained by the convolution of the KKP FFs at $Q_0 = 2$ GeV and the DGLAP FFs. This method for the pp FFs reproduces reasonably well the Q -dependence of the KKP FFs [33]. However, the procedure with the same DGLAP FFs for AA and pp collisions is preferable since it guarantees that in the limit of vanishing induced radiation, the medium-modified FFs $D_{h/i}^m$ exactly reduce to the pp FFs. We calculate the FFs $D_{j/k}^{in}$ from the one gluon induced spectrum accounting for multiple gluon emission in the approximation of independent gluon radiation [35]. The formulas for calculation of the gluon induced spectrum and the FFs $D_{j/k}^{in}$ are given in appendices A and B. Note that in numerical calculations, instead of performing the convolution of the FFs, as in (7), to use the full FFs $D_{h/i}^m$ in (3), we calculated sequentially the cross sections with the help of formula (3) for the FFs in each of stage.

This is technically more convenient because at each stage we deal with the cross sections which (in logarithmic scales) are smooth functions.

As in [25, 28], we account for the effect of the collisional parton energy loss (which is relatively small [12, 13]) by redefining, in calculating the FFs $D_{j/k}^{in}$, the initial QGP temperature (for each geometry of the jet production) according to the condition

$$\Delta E_{rad}(T_0') = \Delta E_{rad}(T_0) + \Delta E_{col}(T_0), \quad (8)$$

where $\Delta E_{rad/col}$ is the radiative/collisional energy loss, T_0 is the real initial temperature of the QGP, and T_0' is the renormalized temperature. We calculate ΔE_{col} using the Bjorken method [10] with an accurate treatment of kinematics of the binary collisions (the details can be found [12]). The effect of collisional energy loss on jet quenching is relatively small. For RHIC the collisional mechanism reduces R_{AA} by $\sim 15 - 20\%$ at $p_T \sim 10 - 20$ GeV, and for the LHC energies the reduction of R_{AA} is $\sim 5 - 15\%$ for $p_T \sim 10 - 100$ GeV (the effect becomes smaller at higher p_T).

We evaluate the induced gluon spectrum for the QGP modeled by a system of the static Debye screened color centers [3]. We assume that the number density of the QGP constituents can be obtained from the entropy in the ideal gas model. The assumption that $n \propto s$ seems to be reasonable, but has no theoretical justification. We perform calculations using the Debye mass obtained in the lattice analysis [36], which gives μ_D/T slowly decreasing with T ($\mu_D/T \approx 3.2$ at $T \sim T_c$, $\mu_D/T \approx 2.4$ at $T \sim 4T_c$). For the T -dependence of the Debye mass we use the temperature extracted from the lattice entropy density obtained in [37]. For a given entropy, this temperature is somewhat larger than the ideal gas temperature (see below). However, for the Debye mass defined via the ideal gas temperature the results do not change significantly. In our calculations of the induced gluon spectrum, we take $m_q = 300$ and $m_g = 400$ MeV for the light quark and gluon quasiparticle masses in the QGP. These values are supported by the analysis of the lattice data within the quasiparticle model [38]. Note that the results are not very sensitive to the gluon mass, and are practically insensitive to the light quark mass.

We perform numerical calculations of the nuclear modification using for the hard cross sections on the right-hand side of (3) the LO pQCD formula with the CTEQ6 [39] parton distribution functions. In calculating the hard cross sections, we use for the virtuality scale in α_s the value cQ with $c = 0.265$ as in the PYTHIA event generator [34], which allows to simulate the higher order effects, and gives a fairly good description of the high- p_T spectra in pp -collisions. Note however that for nuclear modification factor a moderate variation of the hard partonic cross sections is not very crucial. We account for the nuclear modification of the parton distributions with the EPS09 correction [40] (we have found that the difference in the results for EPS09 [40] and EKS98 [41] corrections is visually negligible). In calculating the distribution of the jet production points in the transverse plane in formula (2) and the overlap function T_{AA} in (1), we use the Woods-Saxon nuclear density $\rho_A(r) = \rho_0/[1 + \exp((r - R_A)/d)]$. For Au and Xe nuclei we take $d = 0.54$ fm and $R_A = (1.12A^{1/3} - 0.86/A^{1/3})$ fm as in the GLISSANDO Glauber model

[42] (this gives $R_A \approx 6.37$ and 5.49 fm for Au and Xe, respectively). For Pb nucleus we take the parameters $R_A = 6.62$ and $d = 0.546$ fm as in the PHOBOS Glauber model [43, 44].

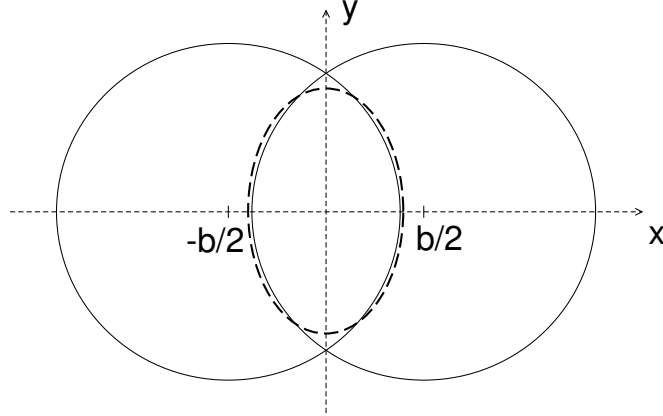


Figure 1. Schematic representation of the fireball geometry in the transverse plane for AA-collision with impact parameter b . See main text for details.

We calculate both radiative and collisional energy loss with running α_s frozen at low momenta at some value α_s^{fr} :

$$\alpha_s(Q^2) = \begin{cases} \alpha_s^{fr} & \text{if } Q \leq Q_{fr} , \\ \frac{4\pi}{9 \log(Q^2/\Lambda_{QCD}^2)} & \text{if } Q > Q_{fr} , \end{cases} \quad (9)$$

where $Q_{fr} = \Lambda_{QCD} \exp \{2\pi/9\alpha_s^{fr}\}$ (in the present analysis we take $\Lambda_{QCD} = 200$ MeV).

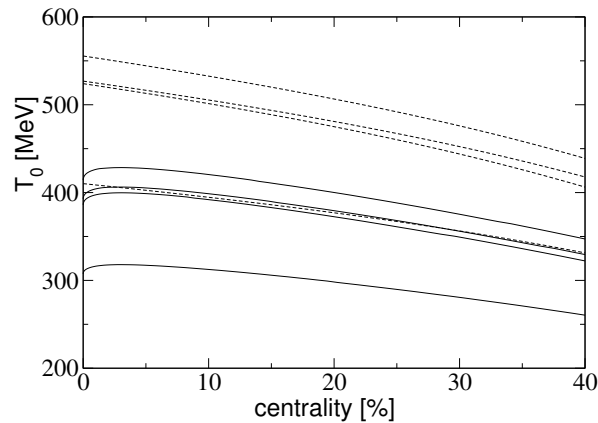


Figure 2. Centrality dependence of the initial QGP temperature obtained in the Glauber model via the average entropy density (solid) and the maximal one at the center of the fireball (dashed) for (from bottom to top): 0.2 TeV Au+Au, 5.44 TeV Xe+Xe, 2.76 and 5.02 TeV Pb+Pb collisions.

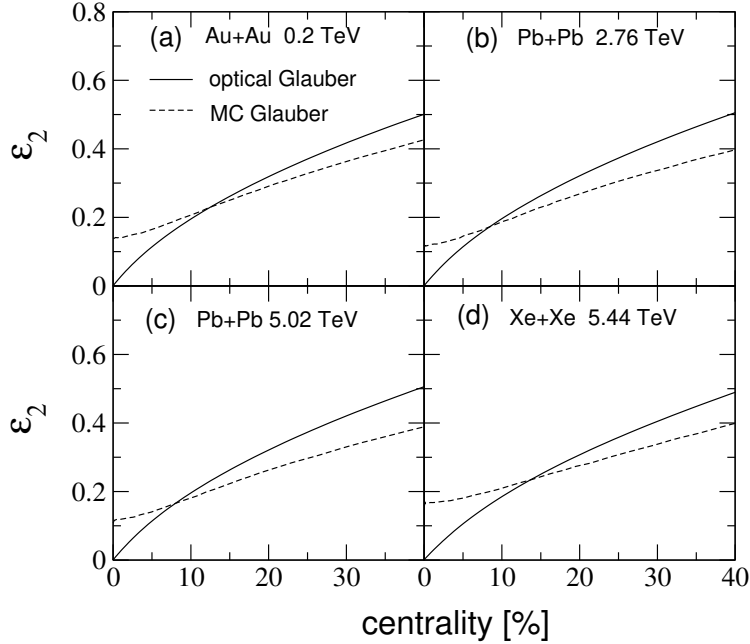


Figure 3. Centrality dependence of the initial fireball eccentricity obtained in the optical (solid) and Monte-Carlo (dashed) Glauber model for: 0.2 TeV Au+Au collisions (a); 2.76 (b) and 5.02 TeV (c) Pb+Pb collisions; 5.44 TeV Xe+Xe collisions (d).

For gluon emission in vacuum the value of α_s^{fr} can be estimated from the relation

$$\frac{1}{\pi} \int_0^2 \text{GeV} dQ \alpha_s(Q) \approx 0.38, \quad (10)$$

obtained in [45] from the heavy quark energy loss. It gives $\alpha_s^{fr} \approx 1.05$. The constraint on α_s^{fr} in vacuum from (10) agrees well with the value of α_s^{fr} obtained from the dipole BFKL analysis of the low- x structure functions [46]. This analysis gives $\alpha_s^{fr} \approx 0.7 - 0.8$ for $\Lambda_{QCD} = 0.3$, which for $\Lambda_{QCD} = 0.2$ corresponds to $\alpha_s^{fr} \approx 1$. In the QGP the thermal effects can suppress the in-medium QCD coupling, and it is reasonable to view α_s^{fr} as a free parameter. Since we fix the quasiparticle masses $m_{g,q}$, and the temperature dependence of the Debye mass, α_s^{fr} is the only free parameter in our calculations.

2.2. Model of the QGP fireball

We perform calculations for the QGP fireball with purely longitudinal Bjorken's 1+1D expansion [16], which gives proper time dependence of the entropy density $s(\tau)/s(\tau_0) = \tau_0/\tau$, where τ_0 is the QGP thermalization time. Under the assumption that the $n \propto s$, we have the same τ -dependence for the number density $n(\tau) = n(\tau_0)\tau_0/\tau$ at $\tau > \tau_0$. For our basic version we take $\tau_0 = 0.5$ fm. However, to understand the sensitivity of the results to τ_0 we also performed the calculations for $\tau_0 = 0.8$ fm. For $\tau < \tau_0$ we take a linear τ -dependence $n(\tau) = n(\tau_0)\tau/\tau_0$. This is just an ad hoc prescription to account for the fact that the medium production is not an instantaneous process. As we said,

we neglect variation of the initial QGP density with the transverse coordinates across the overlapping area of two colliding nuclei. We determine the average initial entropy density of the QGP fireball from the relation [16]

$$s_0 = \frac{C}{\tau_0 S_f} \frac{dN_{ch}^{AA}}{d\eta}. \quad (11)$$

Here S_f is the area of the overlap region of two colliding nuclei (as shown in Fig. 1), and $C = dS/dy / dN_{ch}^{AA}/d\eta \approx 7.67$ [47] is the entropy/multiplicity ratio. We define the overlap region as the overlap of two circles with radius $R = R_A + kd$ with $k = 2$ (R_A and d are the parameters of the Woods-Saxon nuclear density) ‡. We determine the total entropy in the overlap region using the charged hadron multiplicity pseudorapidity density $dN_{ch}/d\eta$ calculated in the Glauber wounded nucleon model [48]. We use the parameters of the model as in our Monte-Carlo Glauber analyses [49, 50], which describe very well data on the midrapidity $dN_{ch}/d\eta$ in 0.2 TeV Au+Au [51], 2.76 [52] and 5.02 TeV [53] Pb+Pb, and 5.44 TeV Xe+Xe [54] collisions. For the ideal gas model the entropy density reads $s(T) = aT^3$ with $a = \frac{4\pi^2}{15} (8/3 + 7N_f/4)$ ($a \approx 18.53$, if one takes $N_f = 2.5$). In Fig. 2 we show the centrality dependence of initial fireball temperature for $\tau_0 = 0.5$ fm for the flat entropy distribution obtained with the help of the relation (11). To illustrate the magnitude of temperature variation in the transverse plane, we also show there the Glauber model predictions for the temperature in the center of the fireball. Note that the ideal gas approximation somewhat underestimates the plasma temperature as compared to that obtained from the lattice entropy density [37] (say, T_{lat} is bigger than that for the ideal gas by $\sim 5 - 10\%$ at $T \sim 300 - 450$, and by $\sim 15 - 25\%$ at $T \sim 150 - 200$ MeV). This fact is not important because in our calculations the ideal gas temperature plays an auxiliary role of a quantity which simply characterizes the entropy density. The crucial point in our scheme, is the assumption that the number density is proportional to the entropy density, and the ratio n/s is the same as for the ideal QGP (see appendix A).

Our calculations show that the azimuthally averaged nuclear modification factor R_{AA} is practically insensitive to the geometry of the fireball. But this is not the case for the flow coefficient v_2 , which to good approximation is proportional to the initial eccentricity ϵ_2 of the fireball. From this point of view, even in the smooth geometry approximation that we use, the model with the almond shaped region with two cups turn out to be too crude because it overestimates ϵ_2 as compared to that calculated with an accurate transverse dependent entropy density. For this reason, we transform the almond shaped interaction region into an elliptic region of the same area (shown by the dashed line in Fig. 1). We will present the results for two variants of the centrality

‡ The value $k \sim 2$ guarantees that for centralities $\lesssim 30\%$, which will be considered in the present analysis, the fraction of the lost jet cross section is negligible. Note, that, in principle, the theoretical predictions for R_{AA} are not very sensitive to variation of R . It is due to a compensation between the enhancement of the energy loss caused by increase of the medium size and its suppression caused by reduction of the medium density.

dependence of ϵ_2 (calculated with the flat entropy density) for the elliptic overlap region. For the first variant we use the optical Glauber model eccentricity ϵ_2 given by

$$\epsilon_2 = \frac{\int dx dy s(x, y)(y^2 - x^2)}{\int dx dy s(x, y)(x^2 + y^2)}. \quad (12)$$

This choice gives ϵ_2 that vanishes as centrality tends to zero. In the second variant we use the rms ϵ_2 (it is often denoted $\epsilon_2\{2\}$) obtained in our previous Monte-Carlo Glauber model simulations [49, 50] of AA -collisions. In this case, due to the density fluctuations, the eccentricity does not vanish at zero centrality. Of course, accurate calculations of the flow coefficients for high- p_T particles require event-by-event simulations which account for fluctuations of the angle between the participant plane (that characterizes the orientation of the fireball ellipse) and the true reaction plane. In the present analysis we ignore the decorrelation between these two planes and simply use the overlap region with fixed orientation (along y -axis as shown in Fig. 1). The inaccuracy of this approximation is connected with incorrect treatment of the mutual geometry of the jet production and soft entropy production. The decorrelation between the geometries of the hard and soft processes can potentially be important at small centralities. However, the jet production is concentrated in the central region of the fireball. For this reason the inaccuracy of the approximation with the fixed fireball ellipse orientation should be small because for jet production at the center of the fireball its orientation becomes unimportant. We checked this by computing R_{AA} and v_2 for different fireball orientations. This test shows that the inaccuracy due to fluctuations of the participant plane should not be bigger 5 – 10% for the flow coefficient v_2 , and negligible for R_{AA} . In Fig. 3 we plot the eccentricity ϵ_2 vs centrality for our two variants. We will perform comparison with experimental data for the region $c < 30\%$, which corresponds to the impact parameter $b \lesssim 1.1R_A$. We do not consider more peripheral collisions because for them the approximation of the flat entropy distribution may become too crude due to enhancement of the boundary effects. Note that in Fig. 3 ϵ_2 for Xe+Xe collisions for the Monte-Carlo variant has been obtained accounting for the prolate shape of the Xe nucleus (see [50] for details), which increases ϵ_2 at $c \sim 0$ by $\sim 15\%$. From Fig. 3 one can see that the Monte-Carlo ϵ_2 becomes smaller than that for the optical Glauber model at $c \gtrsim 10 - 15\%$. This occurs because fluctuations of the nucleon positions in the colliding nuclei increase the width of the almond shaped interaction region when the impact parameter becomes comparable or larger than the nucleus radius.

The medium life/freeze-out time in AA -collisions crucially depends on the transverse QGP expansion, which is neglected in the Bjorken model, but becomes very important at $\tau \gtrsim R_A$ [16, 55]. The pion interferometry at RHIC [56] and LHC [57] energies gives the freeze-out time $\tau_{f.o.} \approx 1.05 \times (dN_{ch}/d\eta)^{1/3}$. We use in our calculations $\tau_{f.o.}$ as the medium life-time, τ_{max} . Note that we use the formulas for the parton energy loss in the QGP. In reality, in the later stage, at τ close to $\tau_{f.o.}$, the hot matter is in the hadron gas phase. However, this fact cannot lead to considerable inaccuracies in the results. The point is that for a given entropy the transport coefficients in the QGP and hadronic gas turn out to be close to each other [58]. And since we use the QGP

number density $\propto s$ our formulas should work in the hadron gas stage as well. Anyway, in general, the effect of the later stage with $\tau \sim \tau_{f.o.}$ on the jet modifications is very small. We checked this by performing calculations also for $\tau_{max} = 0.8 \times (dN_{ch}/d\eta)^{1/3}$.

3. Numerical results

3.1. Optimal α_s^{fr} from the χ^2 fit

In our previous jet quenching analysis [25, 28] it was found that the LHC data on R_{AA} for 2.76 TeV Pb+Pb collisions support somewhat smaller value of α_s^{fr} than the RHIC data for 0.2 TeV Au+Au collisions. This conclusion has been made by a simple visual comparison of the theoretical predictions with the data. In the present work we perform a more accurate comparison with data by performing the χ^2 -fitting of R_{AA} . We include only data on R_{AA} because the predictions of the model for R_{AA} are clearly more robust. In particular the results for R_{AA} are practically insensitive to the shape of the fireball. However, as will be seen below our predictions for v_2 are in reasonable agreement with experimental data. We use the data points for centralities smaller than 30%. We include in the χ^2 -fitting data for 0.2 TeV Au+Au collisions at RHIC [59], for 2.76 TeV [60, 61, 62] and 5.02 TeV [63, 64, 65] Pb+Pb, and 5.44 TeV Xe+Xe [66, 67, 68] collisions. For the lower bound on the particle p_T we take $p_{T,min} = 10$ GeV. However, for the PHENIX data [59], which have a small number of the data points with $p_T > 10$ GeV, we also present the results for $p_{T,min} = 7$ GeV. The value $p_{T,min} \sim 10$ GeV seems to be reasonable from the point of view of the applicability conditions for our scheme. Because at lower p_T the leakage of the probability into the unphysical region $\Delta E_{rad} > E$ (see appendix B) may become too strong. Due to larger energy loss, this effect is stronger for gluons. For this reason, the problem especially concerns the LHC energies, where at $p_T \lesssim 10$ GeV the hadron production comes mostly from gluon jets \S . For data on 0.2 TeV Au+Au collisions from PHENIX [59] we include all data points with $p_T > p_{T,min}$. For the LHC data we perform the χ^2 analysis for two versions of the upper p_T -bound: $p_{T,max} = 120$ and 20 GeV. The latter choice corresponds to the p_T -range for the PHENIX data [59], and for this reason seems to be preferable for studying the variation of α_s^{fr} with the QGP density. For each experiment we calculate χ^2 as

$$\chi^2 = \sum_i^N \frac{(f_i^{exp} - f_i^{th})^2}{\sigma_i^2}, \quad (13)$$

where N is the number of the data points, the squared errors include the systematic and statistic errors $\sigma_i^2 = \sigma_{i,stat}^2 + \sigma_{i,sys}^2$.

In Fig. 4 we show the variation of $\chi^2/d.p.$ (χ^2 per data point) with α_s^{fr} in the range from 0.3 to 1.2 for different AA-collisions and experiments (the curves have been obtained for $\tau_{max} = 1.05 \times (dN_{ch}/d\eta)^{1/3}$) and $\tau_0 = 0.5$ fm. In the panel (a) of Fig. 4

\S Note that, without regard to the applicability of our approximations at low p_T , the inclusion of the data points with $p_T \lesssim 7 - 8$ GeV does not make sense, since at such p_T the non-fragmentation contributions, e.g. from the recombination mechanism [69, 70], may become important.

	$\tau_0 = 0.5$ fm			$\tau_0 = 0.8$ fm		
	α_s^{fr}	95% CI	$\chi^2/d.p.$	α_s^{fr}	95% CI	$\chi^2/d.p.$
Au+Au 0.2 TeV, $p_T > 10$ GeV	$0.67_{-0.08}^{+0.137}$	(0.443, >1.2)	0.167	$0.8_{-0.129}^{+0.232}$	(0.472, >1.2)	0.167
Au+Au 0.2 TeV, $p_T > 7$ GeV	$0.676_{-0.037}^{+0.046}$	(0.511, >1.2)	0.196	$0.823_{-0.066}^{+0.083}$	(0.56, >1.2)	0.186
Pb+Pb 2.76 TeV, $10 < p_T < 120$ GeV	$0.427_{-0.004}^{+0.004}$	(0.405, 0.456)	0.81	$0.461_{-0.005}^{+0.005}$	(0.435, 0.498)	0.873
Pb+Pb 2.76 TeV, $10 < p_T < 20$ GeV	$0.436_{-0.005}^{+0.005}$	(0.419, 0.457)	0.965	$0.475_{-0.006}^{+0.007}$	(0.453, 0.503)	1.016
Pb+Pb 5.02 TeV, $10 < p_T < 120$ GeV	$0.42_{-0.005}^{+0.005}$	(0.398, 0.448)	0.95	$0.456_{-0.006}^{+0.007}$	(0.432, 0.49)	1.021
Pb+Pb 5.02 TeV, $10 < p_T < 20$ GeV	$0.43_{-0.006}^{+0.006}$	(0.412, 0.452)	1.01	$0.472_{-0.008}^{+0.009}$	(0.447, 0.506)	1.048
Xe+Xe 5.44 TeV, $10 < p_T < 120$ GeV	$0.42_{-0.006}^{+0.006}$	(0.382, 0.478)	0.518	$0.455_{-0.007}^{+0.009}$	(0.409, 0.537)	0.544
Xe+Xe 5.44 TeV, $10 < p_T < 20$ GeV	$0.428_{-0.007}^{+0.008}$	(0.392, 0.482)	0.267	$0.467_{-0.01}^{+0.011}$	(0.422, 0.548)	0.257
All LHC, $10 < p_T < 120$ GeV	$0.424_{-0.003}^{+0.003}$	(0.4, 0.454)	0.78	$0.459_{-0.004}^{+0.004}$	(0.432, 0.496)	0.836
All LHC, $10 < p_T < 20$ GeV	$0.432_{-0.004}^{+0.004}$	(0.413, 0.457)	0.794	$0.473_{-0.005}^{+0.005}$	(0.447, 0.508)	0.805
RHIC+LHC, $10 < p_T < 120$ GeV	$0.426_{-0.003}^{+0.003}$	(0.405, 0.443)	0.874	$0.462_{-0.004}^{+0.004}$	(0.437, 0.497)	0.904
RHIC+LHC, $10 < p_T < 20$ GeV	$0.436_{-0.004}^{+0.004}$	(0.419, 0.456)	0.967	$0.477_{-0.005}^{+0.005}$	(0.453, 0.51)	0.924

Table 1. Optimal values of α_s^{fr} with 1σ standard error, 95% CI and corresponding $\chi^2/d.p.$ obtained for $\tau_0 = 0.5$ and 0.8 fm at $\tau_{max} = 1.05 \times (dN_{ch}/d\eta)^{1/3}$ for different data sets. For RHIC the χ^2 fits are performed for the R_{AA} data points with $p_T > 10$ and 7 GeV. For LHC the results are presented for $10 < p_T < 120$ GeV and for $10 < p_T < 20$ GeV p_T -ranges.

we compare the $\chi^2/d.p.$ for the PHENIX data for Au+Au collisions (obtained for $p_{T,min} = 7$ and 10 GeV) with that obtained for all the LHC data for $10 < p_T < 120$ and $10 < p_T < 20$ GeV. In the panels b, c, d we plot separately $\chi^2/d.p.$ for 2.76 and 5.02 TeV Pb+Pb, and 5.44 TeV Xe+Xe collisions (there we show $\chi^2/d.p.$ for each experiment separately and the combined $\chi^2/d.p.$). In calculating χ^2 we have used the theoretical R_{AA} obtained with the help of a cubic spline interpolation for a grid with step $\Delta\alpha_s^{fr} = 0.05$ at $0.3 < \alpha_s^{fr} < 0.5$, and with $\Delta\alpha_s^{fr} = 0.1$ at $0.5 < \alpha_s^{fr} < 1.2$. We also performed the χ^2 fit for $\tau_0 = 0.8$ fm. The optimal values of α_s^{fr} and corresponding values of $\chi^2/d.p.$ for both the versions are summarized in Table I. For the LHC data we present α_s^{fr} and $\chi^2/d.p.$ separately for each energy (and process) and the combined $\chi^2/d.p.$ for all LHC experiments. In Table I we also present the results for all the data sets (RHIC plus LHC). Note that we have checked that the fits with $p_{T,min} \sim 7-8$ GeV for the LHC data give results very similar to that for $p_{T,min} = 10$ GeV. But the robustness of the results in this case may be lower than for $p_{T,min} = 10$ GeV due to possibly larger theoretical uncertainties and the contributions from the non-fragmentation mechanisms [69, 70]. In Table I we present the values of α_s^{fr} with the standard errors (i.e. corresponding to $\Delta\chi^2 = 1$). Also, we give there the 95% confidence intervals (CIs) corresponding to $\Delta\chi^2$ for the 95% quantile of the χ^2 -distribution. The CIs are more appropriate characteristics for understanding the difference between the values of α_s^{fr} for RHIC and LHC.

The results for Pb+Pb collisions are obtained for the Woods-Saxon parameters used in the PHOBOS Glauber model [43]. To understand the sensitivity of the results to the choice of the Woods-Saxon parameters we have also performed calculations for $R_A = 6.49$ and $d = 0.54$ as in the GLISSANDO Glauber model [42]. For this set we have obtained the optimal α_s^{fr} that are smaller only by ~ 0.01 .

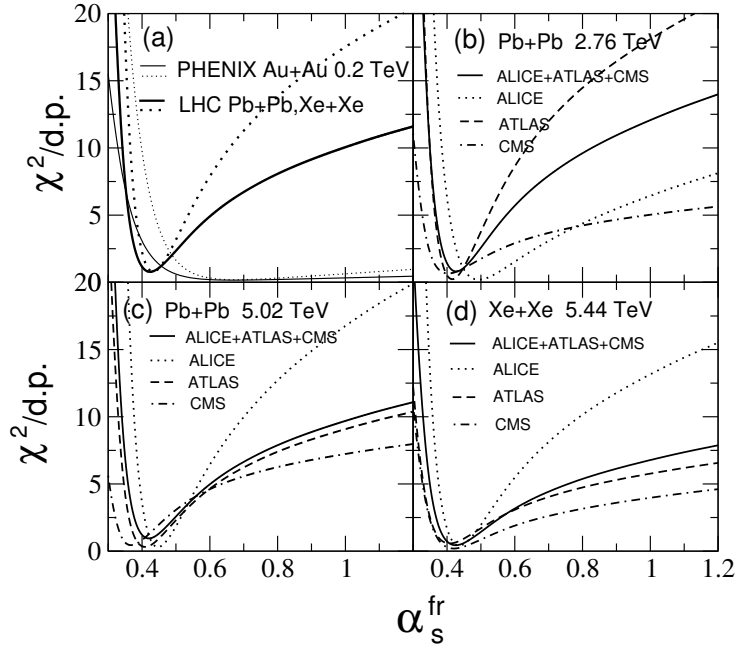


Figure 4. The $\chi^2/d.p.$ vs α_s^{fr} obtained for $c < 30\%$ for the version with $\tau_0 = 0.5$ fm using the RHIC and LHC R_{AA} data: (a) for π^0 at $p_T > 10$ GeV (solid line) and $p_T > 7$ GeV (dotted line) in 0.2 TeV Au+Au collisions from PHENIX [59] and for h^\pm for $10 < p_T < 120$ GeV (thick solid line) and for $10 < p_T < 20$ GeV (thick dotted line) from the LHC for 2.76 TeV (from ALICE [60], ATLAS [61], and CMS [62]) and 5.02 TeV (from ALICE [63], ATLAS [64], and CMS [65]) Pb+Pb collisions, and for 5.44 TeV Xe+Xe collisions (from ALICE [66], ATLAS [67]) and CMS [68]; (b) for 2.76 TeV Pb+Pb collisions for the range $10 < p_T < 120$ GeV; (c) same as (b) for 5.02 TeV; (d) same as (b) for 5.44 TeV Xe+Xe collisions.

From Table I it is seen that for all the data sets we have a good fit quality ($\chi^2/d.p. \lesssim 1$). From Fig. 4 and Table I one can see that for experimental data from LHC the optimal values of α_s^{fr} for different energies/processes turn out to be very similar, but they are noticeably smaller than the optimal α_s^{fr} for Au+Au collisions at RHIC. The values α_s^{fr} for the joint fits of the RHIC and LHC data turn out to be close to that for the LHC data. This occurs because the number of the LHC data points is considerably larger than for the RHIC data. Note, although the values of $\chi^2/d.p.$ for the combined fits (RHIC plus LHC) are quite good ($\chi^2/d.p. < 1$), the quality of the fits for the RHIC data taken separately are not good (for $\tau_0 = 0.5$ fm $\chi^2/d.p. \approx 1.7$ and 2 for $p_{T,max} = 20$ and 120 GeV for the LHC set, respectively). For $\tau_0 = 0.5(0.8)$ fm we have $\alpha_s^{fr}(\text{RHIC})/\alpha_s^{fr}(\text{LHC}) \approx 1.58(1.74)$ for the LHC p_T -region $10 < p_T < 120$ GeV. The situation remains practically the same for the narrow LHC p_T -region (as for the PHENIX data on Au+Au collisions) $10 < p_T < 20$ GeV, which gives $\alpha_s^{fr}(\text{RHIC})/\alpha_s^{fr}(\text{LHC}) \approx 1.55(1.69)$. These ratios will be a bit larger if we use $\alpha_s^{fr}(\text{RHIC})$ for the fit with $p_{T,min} = 7$ that gives slightly bigger values of α_s^{fr} (see Table I). The difference between the optimal values of α_s^{fr} for RHIC and LHC is well seen

from comparison of the CIs for RHIC and LHC. From Table I it is well seen that the the 95% CIs for RHIC and LHC have very small overlaps||. We checked that the 68% CIs for the RHIC and LHC data sets do not overlap at all. These facts say that the difference between the values of α_s^{fr} for RHIC and LHC is a statistically significant effect. Thus, similarly to our previous analyses [26, 28] with visual comparison of the theoretical predictions for R_{AA} with data from RHIC and LHC, the present analysis, with accurate χ^2 -fitting, demonstrates a significant reduction of the in-medium QCD coupling from RHIC to LHC.

Note that the values of $\chi^2/d.p.$ for $\tau_0 = 0.5$ and 0.8 fm presented in Table I are very similar. This says that jet quenching has rather weak sensitivity to the medium formation time, and cannot constrain the value of τ_0 . Below we demonstrate this fact by plotting the predictions for R_{AA} for our two choices of τ_0 . Physically, the fact that jet quenching is weakly sensitive to the initial stage of the medium evolution is due to strong suppression of the induced gluon emission by the finite-size effects in the regime when the the effective gluon formation length is small as compared to the medium thickness [20]. It is worth noting that if the thermalization time decreases with increasing temperature (say, if $\tau_0 \propto 1/T_0$), then it is natural to calculate the ratio $\alpha_s^{fr}(\text{RHIC})/\alpha_s^{fr}(\text{LHC})$ using for RHIC and LHC the values of α_s^{fr} obtained for $\tau_0 = 0.8$ and 0.5 fm, respectively. In this case for the range $10 < p_T < 20$ GeV one obtains $\alpha_s^{fr}(\text{RHIC})/\alpha_s^{fr}(\text{LHC}) \approx 1.85$.

3.2. Comparison with experimental data

In Figs. 5–12 we compare our results for R_{AA} and v_2 with data from: PHENIX for π^0 -meson in 0.2 TeV Au+Au collisions [59, 71]; ALICE [60, 72], ATLAS [61, 73], and CMS [62, 74] for h^\pm in 2.76 TeV Pb+Pb collisions; ALICE [63], ATLAS [64, 75], and CMS [65, 76] for h^\pm in 5.02 TeV Pb+Pb collisions; ALICE [66, 77], ATLAS [67, 78], and CMS [68, 79] for h^\pm in 5.44 TeV Xe+Xe collisions. For each energy/process we show the results obtained with the optimal value of α_s^{fr} for $\tau_0 = 0.5$ fm. To illustrate the sensitivity of R_{AA} to the value of τ_0 , we present the results for $\tau_0 = 0.5$ and 0.8 fm. For R_{AA} we show the predictions for the initial eccentricity ϵ_2 of the fireball obtained in the optical Glauber model. The theoretical curves for R_{AA} for ϵ_2 obtained in the Monte-Carlo Glauber model are indistinguishable from that for the optical Glauber model version of ϵ_2 . For the flow coefficient v_2 , where the results for the two versions of ϵ_2 differ significantly, we plot the predictions for both the choices of ϵ_2 . Note that the results for LHC, shown in Figs. 7–12, are very close to that for the optimal α_s^{fr} for the combined LHC data set and for the combined RHIC plus LHC data set (not shown). In Fig. 5, to visualize better the difference between the predictions for RHIC and LHC, in addition to predictions for R_{AA} in Au+Au collisions obtained with $\alpha_s^{fr} = 0.67$ fitted to the PHENIX data, we also plot the results for $\alpha_s^{fr} = 0.424$ (dashed lines) which is

|| Note that for the investigate region $0.3 < \alpha_s^{fr} < 1.2$ the upper boundaries of the 95% CIs for RHIC are not reached. However, this fact is immaterial from the point of view of the overlap of the CIs for RHIC and LHC.

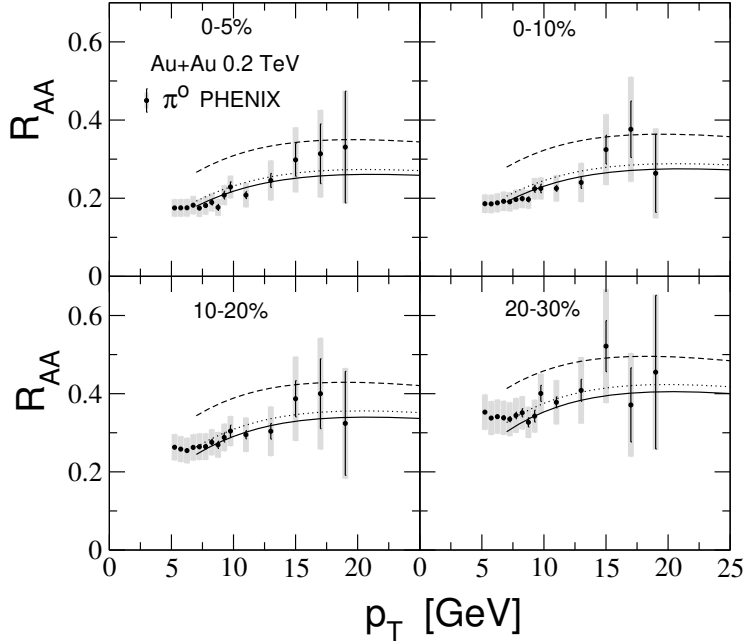


Figure 5. R_{AA} of π^0 for 0.2 TeV Au+Au collisions from our calculations for $\tau_0 = 0.5$ (solid) and 0.8 fm (dotted) compared to data from PHENIX [59]. The solid and dotted curves are for $\alpha_s^{fr} = 0.67$ obtained by fitting R_{AA} in the range $p_T > 10$ GeV for the version with $\tau_0 = 0.5$ fm, and the dashed curves are for $\alpha_s^{fr} = 0.424$ obtained by fitting the LHC data on R_{AA} .

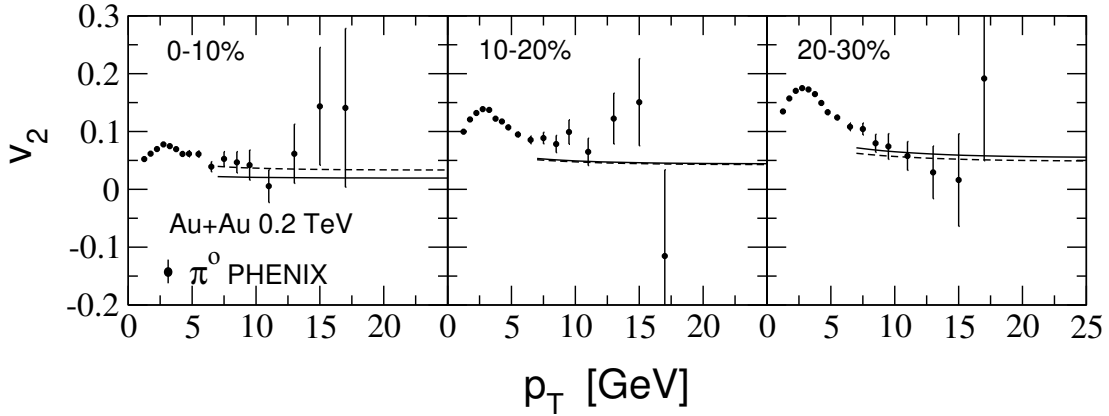


Figure 6. v_2 of π^0 for 0.2 TeV Au+Au collisions obtained for $\tau_0 = 0.5$ with $\alpha_s^{fr} = 0.67$ for the initial fireball eccentricity ϵ_2 calculated in the optical (solid) and Monte-Carlo (dashed) Glauber model (see text for details). Data points are from PHENIX [71].

fitted to the LHC data. As one can see the dashed lines disagree substantially with the experimental R_{AA} . The disagreement is especially strong for $p_T \lesssim 15$ GeV where the errors become relatively small. Note that the same situation occurs for the curves for the combined RHIC plus LHC fit (not shown), which practically coincide with the dashed lines.

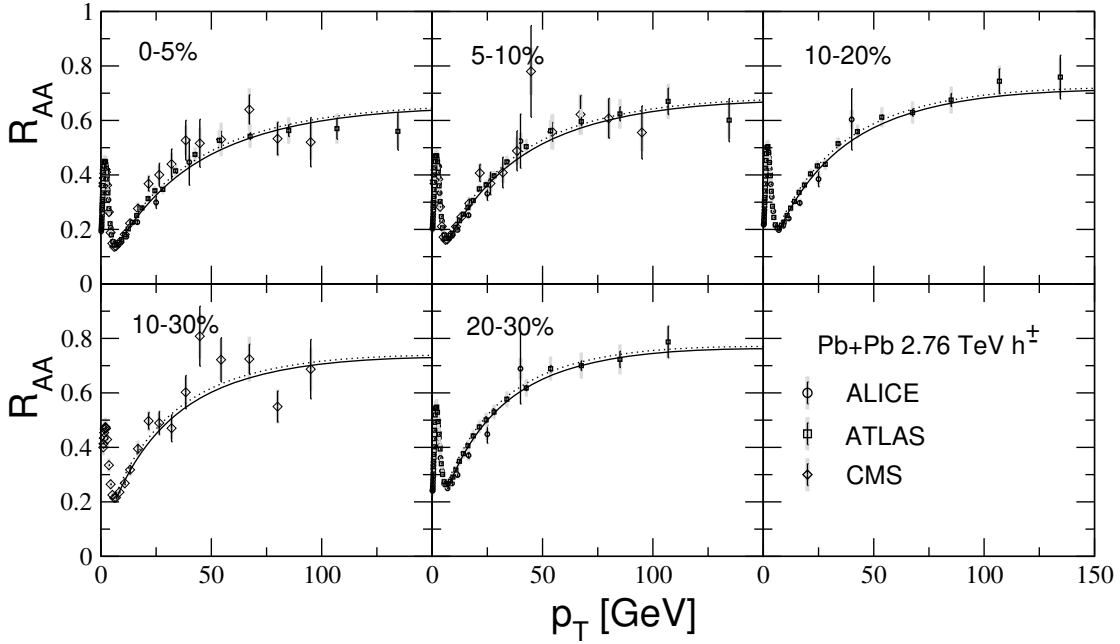


Figure 7. R_{AA} of charged hadrons for 2.76 TeV Pb+Pb collisions from our calculations for $\tau_0 = 0.5$ (solid) and 0.8 fm (dotted) with $\alpha_s^{fr} = 0.427$ obtained by fitting R_{AA} in the range $10 < p_T < 120$ GeV for $\tau_0 = 0.5$ fm. Data points are from ALICE [60], ATLAS [61], and CMS [62].

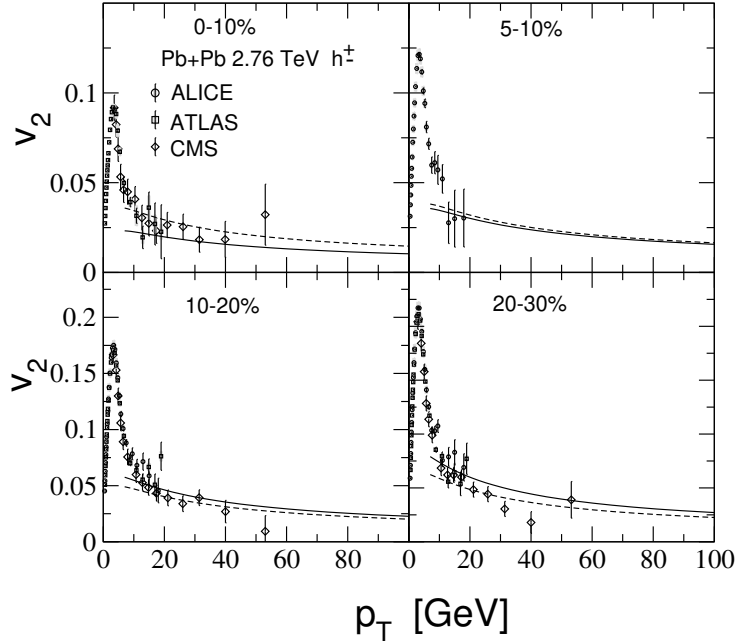


Figure 8. v_2 of charged hadrons in 2.76 TeV Pb+Pb collisions for $\tau_0 = 0.5$ for the initial fireball eccentricity ϵ_2 calculated in the optical (solid) and Monte-Carlo (dashed) Glauber model, $\alpha_s^{fr} = 0.427$ is obtained from the fit of R_{AA} in the range $10 < p_T < 120$ GeV. Data points are from ALICE [72], ATLAS [73], and CMS [74].

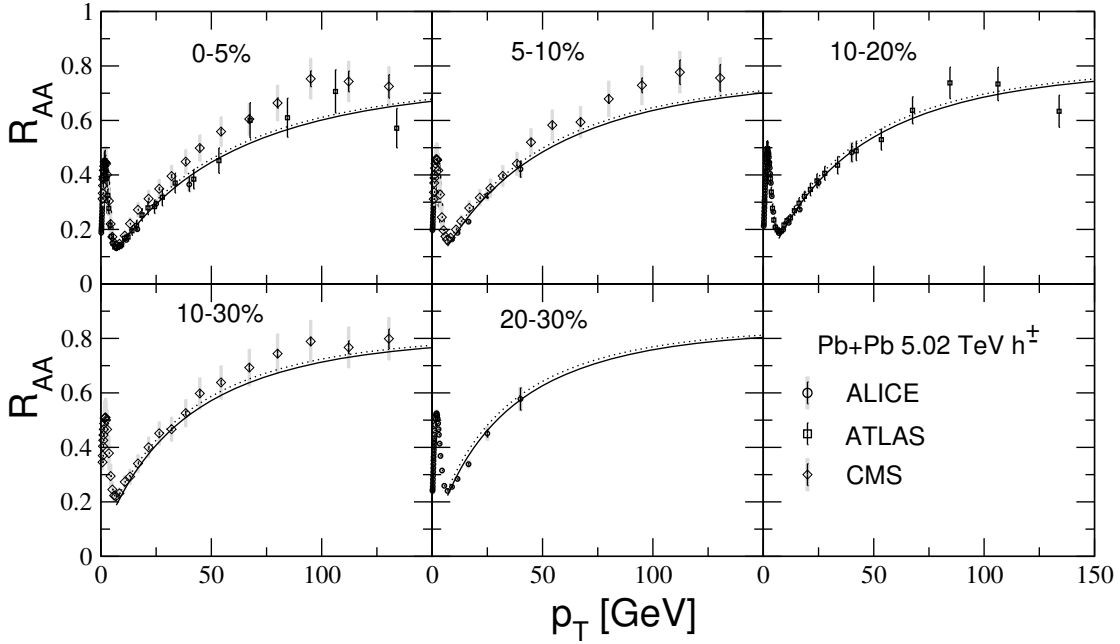


Figure 9. Same as in Fig. 7 for $\sqrt{s} = 5.02$ TeV for the optimal parameter $\alpha_s^{fr} = 0.42$. Data points are from ALICE [63], ATLAS [64], and CMS [65].

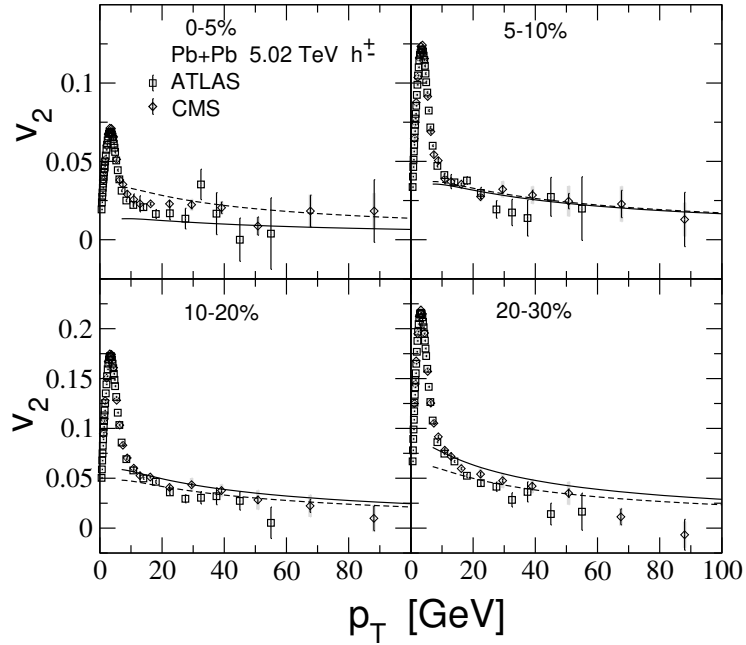


Figure 10. Same as in Fig. 8 for $\sqrt{s} = 5.02$ TeV for $\alpha_s^{fr} = 0.42$. Data points are from ATLAS [75] and CMS [76].

From Figs. 5, 7, 9, 11 one can see that the theoretical predictions for R_{AA} are in quite good agreement with experimental data. One can see that the difference

¶ Note that agreement with the LHC data on R_{AA} in 2.76 TeV 0 – 5% Pb+Pb collisions is somewhat

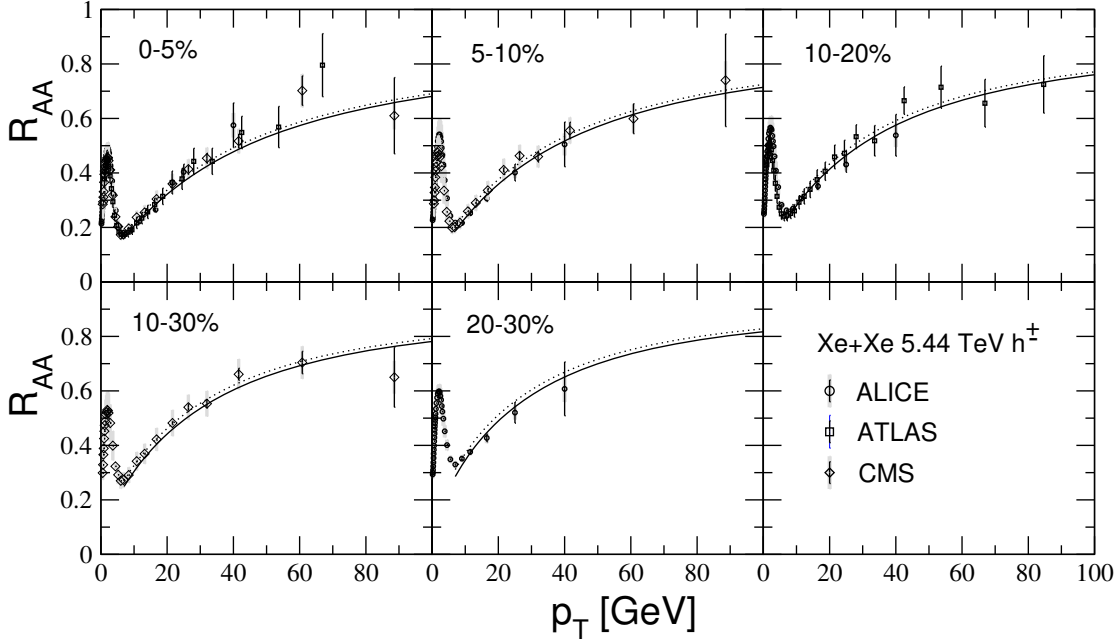


Figure 11. Same as in Fig. 7 for 5.44 TeV Xe+Xe collisions for the optimal parameter $\alpha_s^{fr} = 0.425$. Data points are from ALICE [66], ATLAS [67], and CMS [68].

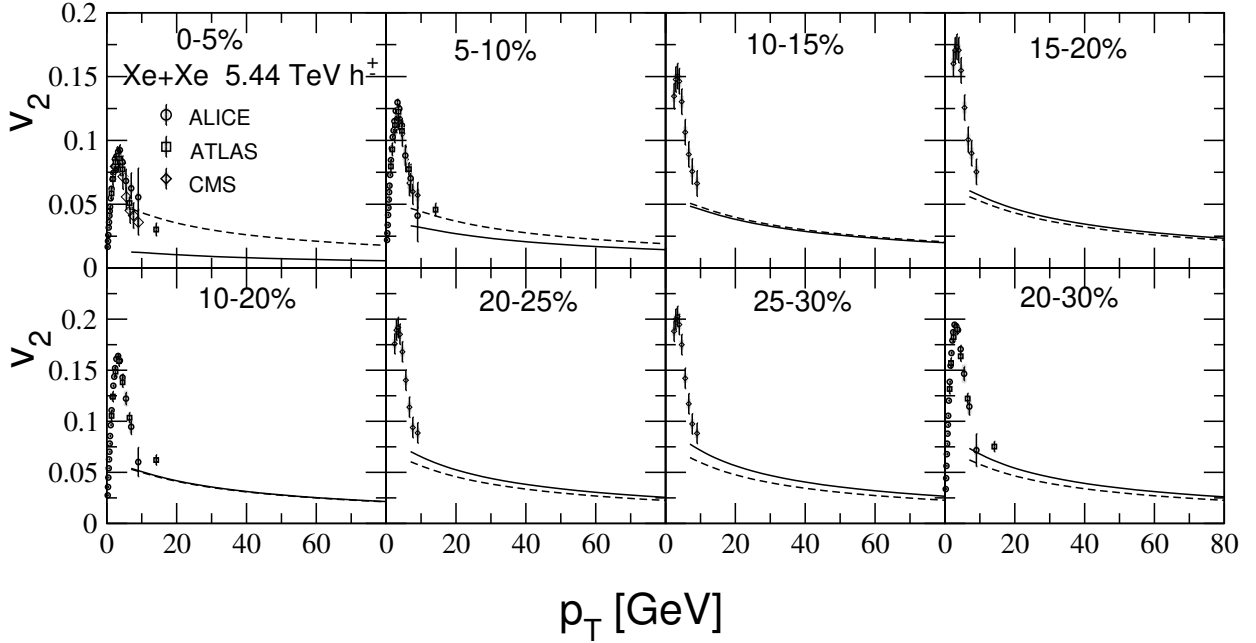


Figure 12. Same as in Fig. 8 for 5.44 TeV Xe+Xe collisions for $\alpha_s^{fr} = 0.425$. Data points are from ALICE [77], ATLAS [78], and CMS [79].

better than in our previous analysis [28]. This is mostly due to use in the present calculations of $\Lambda_{QCD} = 200$ MeV, which leads to a bit steeper rise of R_{AA} at $p_T \gtrsim 20$ GeV as compared to $\Lambda_{QCD} = 300$ MeV used in [28]. Also, in the present analysis we use a physically more reasonable algorithm for

between our results for R_{AA} obtained with $\tau_0 = 0.5$ and 0.8 fm turns out to be very small (especially for LHC energies). Note that although we have not included data on the flow coefficient v_2 into our χ^2 analysis, the theoretical predictions for v_2 are in not bad agreement with the data. Unfortunately, for the PHENIX v_2 data [71] large error bars at $p_T \gtrsim 10$ GeV render difficult a conclusive comparison, but within the errors the calculations are consistent with the data. The situation is better for the LHC measurements of v_2 in 2.76 and 5.02 TeV Pb+Pb collisions (they give v_2 up to $p_T \sim 50 - 90$ GeV). For Pb+Pb collisions we obtain somewhat better agreement with the LHC v_2 data for the Monte-Carlo version of the initial eccentricity ϵ_2 (see Figs. 8, 9). However, for the optical Glauber model version the agreement with data is also quite reasonable. The major difference between the two versions is that the Monte-Carlo version gives a significantly larger value of v_2 for $c \lesssim 5\%$. For 5.44 Xe+Xe collisions the available data on v_2 are restricted to the region $p_T \lesssim 14$ GeV, and a comparison of the theoretical p_T -dependence of v_2 with experiment is impossible. But nevertheless, from Fig. 12 one can see that our curves have reasonable matches to the experimental data points at $p_T \sim 10$ GeV.

The fact that our predictions for v_2 are in a reasonable agreement with data at $c \sim 20 - 30\%$ says that it describes correctly the L -dependence of the parton energy loss in the QGP. Indeed, for such centralities the typical parton path length in the fireball (see Fig. 1) for parton momentum along the y -axis is bigger than that in the case of x -axis by a factor of $\sim 1.3 - 1.4$, and to describe the v_2 data the model should reproduce correctly the difference in parton energy losses for these two geometries. This can also be concluded from description of the difference between R_{AA} for Pb+Pb and Xe+Xe collisions because the Pb nucleus radius is larger than that for the Xe nucleus by a factor of ~ 1.18 .

The curves shown in Figs. 5–12 are obtained for $\tau_{max} = \tau_{f.o} = 1.05 \times (dN_{ch}/d\eta)^{1/3}$ [56, 57]. To check the sensitivity to τ_{max} , we also performed calculations for $\tau_{max} = 0.8 \times (dN_{ch}/d\eta)^{1/3}$. We obtained very small difference between the two versions for the LHC energies. For RHIC the latter version gives R_{AA} larger by $\sim 3 - 5\%$ at $p_T \sim 10 - 20$ GeV. Thus, we see that jet quenching is rather weakly sensitive to the very initial and the very late stages of the QCD matter evolution.

Altogether, our calculations show that the pQCD picture can give a quite good agreement with the jet quenching data from RHIC and LHC. However, in the present formulation the simultaneous description of the RHIC and LHC data requires to use different α_s^{fr} at RHIC and LHC energies. A similar difference between jet quenching at RHIC and LHC energies, in terms of the transport coefficient \hat{q} , has been found in [80, 81]. From the point of view of the QCD matter produced in AA -collisions, the difference in the optimal α_s^{fr}/\hat{q} for RHIC and LHC may be due somewhat stronger thermal suppression of the effective QCD coupling at the LHC energies. In order to draw

accounting for the leakage of the probability into unphysical region $\Delta E_{rad} > E$ in calculating the induced FFs (see appendix B for details). This somewhat reduces R_{AA} at $p_T \lesssim 15$ GeV for the LHC energies.

a firm conclusion on this possibility it is highly desirable to perform calculations with a temperature/density dependent α_s . We leave this to a future analysis. It is also possible that the bigger values of α_s^{fr}/\hat{q} for RHIC mimic an enhancement of parton rescatterings in the later low temperature stage of the QGP evolution, which should play a more important role at RHIC energies. This may be due to presence in the QGP at $T \sim T_c$ [82] of the nonperturbative objects like color-magnetic monopoles, which can enhance the induced gluon emission [83, 84]. Another cause of the reduction of α_s^{fr} at the LHC energy may be related to formation of the mini-QGP in pp -collisions [86, 85], which was ignored in the present analysis. If the mini-QGP formation occurs in pp -collisions, the effective nuclear modification factor turns out to be enhanced by a factor $1/R_{pp}$ (see [85] for details), where R_{pp} is the modification factor describing jet quenching in the mini-QGP in pp -collisions. Since jet quenching in the mini-QGP should be stronger at the LHC energies, the effect of the $1/R_{pp}$ factor should be stronger at the LHC energies. This fact should reduce the difference between the values of α_s^{fr} for RHIC and LHC. Note that, if we assume that the mini-QGP is formed only at the LHC energies, then it is enough to have for LHC $R_{pp} \sim 0.8 - 0.85$ (such values seems to be very realistic [85]) at $p_T \sim 10 - 20$ GeV to obtain very similar values of α_s^{fr} for RHIC and LHC.

In principle, the optimal values of α_s^{fr} for the RHIC and LHC energies might be affected by the transverse flow effects, which are neglected in our calculations. The transverse expansion becomes very important at later stages ($\tau \gtrsim R_A$) of the QGP evolution [16, 87, 88], and it is somewhat stronger at the LHC energies. But the possibility that $\alpha_s^{fr}(\text{RHIC})/\alpha_s^{fr}(\text{LHC}) > 1$ is due to different magnitude of the transverse flow at RHIC and LHC seems to be unrealistic because, as we mentioned above, the effect of the later stage on R_{AA} is rather small⁺. To understand better whether this scenario is possible, we have performed calculations using for RHIC the value of τ_{max} corresponding to 2.76 TeV Pb+Pb collisions (which is bigger by a factor of ~ 1.33). Even for this unrealistic scenario, we obtained the optimal value $\alpha_s^{fr} \approx 0.658$ (for $\tau_0 = 0.5$ fm), which is very close to that given in table I. This test shows that the possibility that $\alpha_s^{fr}(\text{RHIC})/\alpha_s^{fr}(\text{LHC}) > 1$ is due to ignoring the transverse flow seems to be highly unrealistic.

4. Conclusions

In this paper we have performed a detailed comparison of the pQCD jet quenching calculations with experimental data on the nuclear modification factor R_{AA} and the flow coefficient v_2 for light hadrons from RHIC and LHC including the newly available LHC data for 5.44 TeV Xe+Xe collisions. The calculations are performed within the LCPI [6] approach using the method suggested in [30, 25]. We account for radiative and collisional energy loss, and fluctuations of the jet path lengths in the QGP. The

⁺ In principle, as was shown in [89] (see also [90]), the effect of the radial flow on R_{AA} is relatively small. This occurs due to a considerable compensation between enhancement of the energy loss caused by increase of the medium size and its suppression caused by reduction of the medium density.

calculations are performed with running α_s frozen at low momenta at some value α_s^{fr} , which is treated as a free parameter. We have determined the optimal values of α_s^{fr} from the χ^2 fit of R_{AA} . We have found that for the QGP formation time $\tau_0 = 0.5$ fm the RHIC data on R_{AA} in Au+Au collisions give the optimal value $\alpha_s^{fr}(\text{RHIC}) \approx 0.67$, while the LHC data give $\alpha_s^{fr}(\text{LHC}) \approx 0.42$. The 95% CIs for $\alpha_s^{fr}(\text{RHIC})$ and $\alpha_s^{fr}(\text{LHC})$ have a very narrow overlap region, and the 68% CIs do not overlap at all. This clearly shows that the difference between α_s^{fr} for RHIC and LHC is statistically significant. For the optimal values of α_s^{fr} our predictions for R_{AA} are in quite good agreement with experiment. Our χ^2 fitting of R_{AA} for all the data sets gives $\chi^2/d.p. \lesssim 1$. For the flow coefficient v_2 , which was not included in the χ^2 analysis, our predictions are in reasonable agreement with the data as well. The fact that the model describes well R_{AA} simultaneously for Pb+Pb and Xe+Xe collisions, and is in reasonable agreement with data on v_2 at $c \sim 20 - 30\%$ says that the model correctly reproduces the L -dependence of the parton energy loss. Our calculations show that jet quenching is not very sensitive to the initial and final times of the QGP evolution.

The difference between the optimal values of α_s^{fr} for RHIC and LHC (which has been also found in our previous analyses [26, 28]) may be due to a somewhat stronger thermal suppression of the QCD coupling at LHC, or due to a more important role at RHIC of the color-monopole states in the QGP at $T \sim T_c$ [83]. Also, this may be related, at least partly, to the mini-QGP formation in pp -collisions, which should affect differently the predictions for R_{AA} at the RHIC and LHC energies. These questions need further investigations.

I am grateful to O.L. Kodolova for a helpful communication. This work is supported by the Program 0033-2019-0005 of the Russian Ministry of Science and Higher Education.

Appendix A: One gluon spectrum

In this appendix, we give the formulas used for calculation of the induced gluon spectrum. We use the representation for the gluon distribution obtained in [30], which is convenient for numerical calculations. For $q \rightarrow gq$ process the gluon spectrum in $x = E_g/E_q$ reads

$$\frac{dP}{dx} = \int_0^L dz n(z) \frac{d\sigma_{eff}^{BH}(x, z)}{dx}, \quad (\text{A1})$$

where $n(z)$ is the medium number density, $d\sigma_{eff}^{BH}/dx$ is an effective Bethe-Heitler cross section accounting for both the LPM and the finite-size effects. The $d\sigma_{eff}^{BH}/dx$ reads

$$\frac{d\sigma_{eff}^{BH}(x, z)}{dx} = -\frac{P_q^g(x)}{\pi M} \text{Im} \int_0^z d\xi \alpha_s(Q^2(\xi)) \left. \frac{\partial}{\partial \rho} \left(\frac{F(\xi, \rho)}{\sqrt{\rho}} \right) \right|_{\rho=0}. \quad (\text{A2})$$

Here $P_q^g(x) = C_F[1 + (1-x)^2]/x$ is the usual splitting function for $q \rightarrow gq$ process, $M = Ex(1-x)$ is the reduced "Schrödinger mass", $Q^2(\xi) = aM/\xi$ with $a \approx 1.85$ [12], F is the solution to the radial Schrödinger equation for the azimuthal quantum number $m = 1$

$$i \frac{\partial F(\xi, \rho)}{\partial \xi} = \left[-\frac{1}{2M} \left(\frac{\partial}{\partial \rho} \right)^2 + v(\rho, x, z - \xi) + \frac{4m^2 - 1}{8M\rho^2} + \frac{1}{L_f} \right] F(\xi, \rho) \quad (\text{A3})$$

with the boundary condition $F(\xi = 0, \rho) = \sqrt{\rho} \sigma_3(\rho, x, z) \epsilon K_1(\epsilon \rho)$ (K_1 is the Bessel function), $L_f = 2M/\epsilon^2$ with $\epsilon^2 = m_q^2 x^2 + m_g^2 (1-x)^2$, $\sigma_3(\rho, x, z)$ is the cross section of interaction of the $q\bar{q}g$ system with a medium constituent located at z . The potential v in (A3) reads

$$v(\rho, x, z) = -i \frac{n(z) \sigma_3(\rho, x, z)}{2}. \quad (\text{A4})$$

The σ_3 is given by [91]

$$\sigma_3(\rho, x, z) = \frac{9}{8} [\sigma_{q\bar{q}}(\rho, z) + \sigma_{q\bar{q}}((1-x)\rho, z)] - \frac{1}{8} \sigma_{q\bar{q}}(x\rho, z), \quad (\text{A5})$$

where

$$\sigma_{q\bar{q}}(\rho, z) = C_T C_F \int d\mathbf{q} \alpha_s^2(q^2) \frac{[1 - \exp(i\mathbf{q}\boldsymbol{\rho})]}{[q^2 + \mu_D^2(z)]^2} \quad (\text{A6})$$

is the local dipole cross section for the color singlet $q\bar{q}$ pair ($C_{F,T}$ are the color Casimir for the quark and thermal parton (quark or gluon), μ_D is the local Debye mass).

For $g \rightarrow gg$ one should replace the splitting function and m_q by m_g in ϵ^2 . The σ_3 in this case reads

$$\sigma_3(\rho, x, z) = \frac{9}{8} [\sigma_{q\bar{q}}(\rho, z) + \sigma_{q\bar{q}}((1-x)\rho, z) + \sigma_{q\bar{q}}(x\rho, z)]. \quad (\text{A7})$$

As was said in the main text, we assume that the number density of the QGP is proportional to the entropy density. Since $\sigma_{q\bar{q}}$ is proportional to the Casimir operator of the scattering center, one can treat the QGP as a system of the triplet color centers with the number density $n = n_q + n_g C_A/C_F$ (here n_q is the number density of quarks and antiquarks, and n_g is the number density of gluons, C_A and C_F are the gluon and quark Casimir operators). Then, in the ideal gas model, the effective number density n in the potential (A4), which includes both the quark and gluons, can be written as $n(z) = bT^3(z)$ with $b = 9\xi(3)(N_f + 4)/\pi^2 \approx 7.125$ (for $N_f = 2.5$).

Appendix B: Calculation of the induced FFs

In this appendix, we discuss the method for computation of the induced FFs. Let us consider first the case of quark jets. We use the approximation of independent gluon emission [92]. In this approximation the quark distribution in $\xi = \Delta E/E$ in terms of the one gluon spectrum dP/dx can be written as (we omit argument E)

$$W(\xi) = W_0 \sum_{n=1}^{\infty} \frac{1}{n!} \left[\prod_{i=1}^n \int_0^1 dx_i \frac{dP}{dx_i} \right] \delta \left(\xi - \sum_{i=1}^n x_i \right), \quad W_0 = \exp \left[- \int_0^1 dx \frac{dP}{dx} \right], \quad (\text{B1})$$

where W_0 is the no gluon emission probability. At $\xi \ll 1$ the main effect of the multiple gluon emission is the Sudakov suppression, which reflects a simple fact that emission of gluons with the fractional momentum bigger than ξ is forbidden. $W(\xi)$ may be written as [93]

$$W(\xi) = \sum_{n=1}^{\infty} W_n(\xi), \quad (\text{B2})$$

where W_n are determined by the recurrence relations

$$W_{n+1}(\xi) = \frac{1}{n+1} \int_0^\xi dx W_n(\xi-x) \frac{dP}{dx}, \quad W_1(\xi) = W_0 \frac{dP}{d\xi}. \quad (\text{B3})$$

In numerical calculations we set $dP/dx = 0$ at $x < m_g/E_q$ and $1-x < m_q/E_q$.

When the average energy loss is small $\langle \Delta E \rangle / E \ll 1$, one can define the induced $q \rightarrow q$ FF as $D_{q/q}^{in}(z) = W(\xi = 1-z)$. However, for real situation of AA -collisions the ratio $\langle \Delta E \rangle / E$ is not very small, and the above prescription can violate the flavor conservation

$$\int_0^1 dz D_{q/q}^{in}(z) = 1 \quad (\text{B4})$$

due to a leakage of probability into the unphysical region of $\xi > 1$ [93, 18]. One can expect that the inaccuracy of the independent gluon emission picture due to the probability leakage should be concentrated in the region of $\xi \sim 1$. At small ξ the ξ -dependence of $W(\xi)$ comes from the Sudakov suppression. Since it is mostly connected with the one gluon radiation, the approximation of independent gluon emission should work well for $W(\xi)$ at $\xi \ll 1$. For this reason to cure the ‘‘flavor nonconservation’’ it is reasonable to modify somehow $W(\xi)$ only in the region of large ξ . In the present analysis we multiply $W(\xi)$ by a modification factor K_{qq} at $\xi > 0.5$, and determine its value from the flavor conservation (B4).

We account for the $q \rightarrow g$ transition as well. We define the $q \rightarrow g$ FF as

$$D_{g/q}^{in}(z) = K_{gq} dP/dz, \quad (\text{B5})$$

where the coefficient K_{gq} is determined from the momentum sum rule

$$\int_0^1 dz z [D_{q/q}^{in}(z) + D_{g/q}^{in}(z)] = 1. \quad (\text{B6})$$

For gluon we account for only $g \rightarrow g$ transition. We neglect the induced gluon conversion into $q\bar{q}$ pairs, which for light quarks for RHIC and LHC conditions turns out to be relatively small [94]. At $z > 0.5$, similarly to the $q \rightarrow q$ case, we take $D_{g/g}^{in}(z) = W(\xi = 1-z)$, where now $W(\xi)$ is defined via the one gluon spectrum $g \rightarrow gg$. For $g \rightarrow gg$ transition, due to the $x \leftrightarrow 1-x$ symmetry of the function dP/dx , we can use 0.5 for the upper limit in x -integrations in (B1) (we view the softest gluon with $x < 0.5$ as a radiated gluon). In the soft region $z < 0.5$ we take $D_{g/g}(z) = K_{gg} dP/dx$ (with $x = z$). We determine the coefficient $K_{g/g}$ from the the momentum sum rule

$$\int_0^1 dz z D_{g/g}^{in}(z) = 1, \quad (\text{B7})$$

which should be satisfied (if one neglects the $g \rightarrow q\bar{q}$ processes).

Our ansatze on the z -dependence of the induced FFs in the region $z < 0.5$ have not serious theoretical motivations. Fortunately, the form of the induced FFs in the soft region is practically not important because the typical values of z for the induced FFs are very close to unity (say, for Au+Au collisions at 0.2 TeV $\langle z \rangle \sim 0.9 - 0.95$ at $p_T \sim 10 - 20$ GeV). For this reason the soft region plays a minor role.

Note that the algorithm for calculation of the induced FFs given above is somewhat different from that used in [26, 28]. In the present analysis, to ensure the probability and momentum conservation we modify only the FFs in the region $z < 0.5$, while in [26, 28] we performed the renormalization for the whole region of z . The latter method leads to somewhat larger R_{AA} at $p_T \lesssim 20$ GeV due an increase of the gluon contribution (for the quark jets that dominate at RHIC energies the difference between two methods is small). The new algorithm seems to be more physically reasonable because, as we said above, the values of z in the induced FFs that dominate the hadron cross sections are very close to unity, and this region of z should not be affected strongly by the leakage of the probability from the region $z \sim 0.5$.

References

- [1] U.A. Wiedemann, Landolt-Bornstein **23**, 521 (2010) [arXiv:0908.2306].
- [2] Y. Mehtar-Tani, J.G. Milhano, and K. Tywoniuk, Int. J. Mod. Phys. **A28**, 1340013 (2013) [arXiv:1302.2579].
- [3] M. Gyulassy and X.N. Wang, Nucl. Phys. **B420**, 583 (1994) [arXiv:nucl-th/9306003].
- [4] R. Baier, Y.L. Dokshitzer, A.H. Mueller, S. Peigné, and D. Schiff, Nucl. Phys. **B483**, 291 (1997) [arXiv:hep-ph/9607355].
- [5] R. Baier, Y.L. Dokshitzer, A.H. Mueller, S. Peigné, and D. Schiff, Nucl. Phys. **B484**, 265 (1997) [arXiv:hep-ph/9608322].
- [6] B.G. Zakharov, JETP Lett. **63**, 952 (1996) [arXiv:hep-ph/9607440].
- [7] U.A. Wiedemann, Nucl. Phys. **A690**, 731 (2001) [arXiv:hep-ph/0008241].
- [8] M. Gyulassy, P. Lévai, and I. Vitev, Nucl. Phys. **B594**, 371 (2001) [arXiv:hep-ph/0006010].
- [9] P. Arnold, G.D. Moore, and L.G. Yaffe, JHEP **0206**, 030 (2002) [arXiv:hep-ph/0204343].
- [10] J.D. Bjorken, Fermilab preprint 82/59-THY (1982, unpublished).
- [11] R. Baier, D. Schiff, and B.G. Zakharov, Ann. Rev. Nucl. Part. Sci. **50**, 37 (2000) [arXiv:hep-ph/0002198].
- [12] B.G. Zakharov, JETP Lett. **86**, 444 (2007) [arXiv:0708.0816].
- [13] G.-Y. Qin, J. Ruppert, C. Gale, S. Jeon, G.D. Moore, and M.G. Mustafa, Phys. Rev. Lett. **100**, 072301 (2008) [arXiv:0710.0605].
- [14] R. Baier, Y.L. Dokshitzer, A.H. Mueller, and D. Schiff, Nucl. Phys. **B531**, 403 (1998) [arXiv:hep-ph/9804212].
- [15] R. Baier, Y.L. Dokshitzer, A.H. Mueller and D. Schiff, Phys. Rev. **C58**, 1706 (1998) [arXiv:hep-ph/9803473].
- [16] J.D. Bjorken, Phys. Rev. **D27**, 140 (1983).
- [17] C.A. Salgado and U.A. Wiedemann, Phys. Rev. Lett. **89**, 092303 (2002) [arXiv:hep-ph/0204221].
- [18] K.J. Eskola, H. Honkanen, C.A. Salgado, and U.A. Wiedemann, Nucl. Phys. **A747**, 511 (2005) [arXiv:hep-ph/0406319].
- [19] S.P. Adhya, C.A. Salgado, M. Spousta, and K. Tywoniuk, [arXiv:1911.12193].
- [20] B.G. Zakharov, JETP Lett. **73**, 49 (2001) [arXiv:hep-ph/0012360].

- [21] P.B. Arnold, Phys. Rev. **D80**, 025004 (2009) [arXiv:0903.1081].
- [22] P. Aurenche and B.G. Zakharov, JETP Lett. **90**, 237 (2009) [arXiv:0907.1918].
- [23] S. Shi, J. Liao, M. Gyulassy, Chin. Phys. **C43**, 044101 (2019) [arXiv:1808.05461].
- [24] D. Zigic, B. Ilic, M. Djordjevic, M. Djordjevic, Phys. Rev. **C101**, 064909 (2020) [arXiv:1908.11866].
- [25] B.G. Zakharov, JETP Lett. **88**, 781 (2008) [arXiv:0811.0445].
- [26] B.G. Zakharov, JETP Lett. **93**, 683 (2011) [arXiv:1105.2028].
- [27] B.G. Zakharov, J. Phys. **G38**, 124161 (2011).
- [28] B.G. Zakharov, J. Phys. **G40**, 085003 (2013) [arXiv:1304.5742].
- [29] P. Aurenche and B.G. Zakharov, JETP Lett. **85**, 149 (2007) [arXiv:hep-ph/0612343].
- [30] B.G. Zakharov, JETP Lett. **80**, 617 (2004) [arXiv:hep-ph/0410321].
- [31] S. Caron-Huot and C. Gale, Phys. Rev. **C82**, 064902 (2010) [arXiv:1006.2379].
- [32] W. Broniowski and W. Florkowski, Phys. Rev. **C65**, 024905 (2002) [nucl-th/0110020].
- [33] B.A. Kniehl, G. Kramer, and B. Potter, Nucl. Phys. **B582**, 514 (2000) [arXiv:hep-ph/0010289].
- [34] T. Sjostrand, L. Lonnblad, S. Mrenna, and P. Skands, arXiv:hep-ph/0308153.
- [35] R. Baier, Yu.L. Dokshitzer, A.H. Mueller, and D. Schiff, JHEP **0109**, 033 (2001) [arXiv:hep-ph/0106347].
- [36] O. Kaczmarek and F. Zantow, Phys. Rev. **D71**, 114510 (2005) [arXiv:hep-lat/0503017].
- [37] S. Borsanyi, G. Endrodi, Z. Fodor, A. Jakovac, S.D. Katz, S. Krieg, C. Ratti, and K. K. Szabo, JHEP **1011**, 077 (2010) [arXiv:1007.2580].
- [38] P. Lévai and U. Heinz, Phys. Rev. **C57**, 1879 (1998) [hep-ph/9710463].
- [39] S. Kretzer, H.L. Lai, F. Olness, and W.K. Tung, Phys. Rev. **D69**, 114005 (2004).
- [40] K.J. Eskola, H. Paukkunen, and C.A. Salgado, JHEP **0904**, 065 (2009) [arXiv:0902.4154].
- [41] K.J. Eskola, V.J. Kolhinen, and C.A. Salgado, Eur. Phys. J. **C9**, 61 (1999) [arXiv:hep-ph/9807297].
- [42] M. Rybczynski, G. Stefanek, W. Broniowski, and P. Bozek, Comput. Phys. Commun. **185**, 1759 (2014) [arXiv:1310.5475].
- [43] B. Alver, M. Baker, C. Loizides, and P. Steinberg, arXiv:0805.4411.
- [44] H. De Vries, C.W. De Jager, and C. De Vries, Atomic Data and Nuclear Data Tables **36**, 495 (1987).
- [45] Yu.L. Dokshitzer, V.A. Khoze, and S.I. Troyan, Phys. Rev. **D53**, 89 (1996) [arXiv:hep-ph/9506425].
- [46] N.N. Nikolaev and B.G. Zakharov, Phys. Lett. **B327**, 149 (1994) [arXiv:hep-ph/9402209].
- [47] B. Müller and K. Rajagopal, Eur. Phys. J. **C43**, 15 (2005) [arXiv:hep-ph/0502174].
- [48] D. Kharzeev and M. Nardi, Phys. Lett. **B507**, 121 (2001) [arXiv:nucl-th/0012025].
- [49] B.G. Zakharov, JETP **124**, 860 (2017) [arXiv:1611.05825].
- [50] B.G. Zakharov, Eur. Phys. J. **C78**, 427 (2018) [arXiv:1804.05405].
- [51] B.I. Abelev *et al.* [STAR Collaboration], Phys. Rev. **C79**, 034909 (2009) [arXiv:0808.2041].
- [52] K. Aamodt *et al.* [ALICE Collaboration], Phys. Rev. Lett. **106**, 032301 (2011) [arXiv:1012.1657].
- [53] J. Adam *et al.* [ALICE Collaboration] Phys. Rev. Lett. **116**, 222302 (2016), [arXiv:1512.06104].
- [54] S. Acharya *et al.* [ALICE Collaboration], Phys. Lett. **B790**, 35 (2019) [arXiv:1805.04432].
- [55] A. Kisiel, W. Broniowski, M. Chojnacki, and W. Florkowski, Phys. Rev. **C79**, 014902 (2009) [arXiv:0808.3363].
- [56] J. Adams *et al.* [STAR Collaboration], Phys. Rev. **C71**, 044906 (2005) [nucl-ex/0411036].
- [57] J. Adam *et al.* [ALICE Collaboration] Phys. Rev. **C93**, 024905(2016) [arXiv:1507.06842].
- [58] R. Baier, Nucl. Phys. **A715**, 209 (2003) [hep-ph/0209038].
- [59] A. Adare *et al.* [PHENIX Collaboration], Phys. Rev. **C87**, 034911 (2013) [arXiv:1208.2254].
- [60] B. Abelev *et al.* [ALICE Collaboration], Phys. Lett. **B720**, 52 (2013) [arXiv:1208.2711].
- [61] G. Aad *et al.* [ATLAS Collaboration], JHEP **1509**, 050 (2015) [arXiv:1504.04337].
- [62] S. Chatrchyan *et al.* [CMS Collaboration], Eur. Phys. J. **C72**, 1945 (2012) [arXiv:1202.2554].
- [63] S. Acharya *et al.* [ALICE Collaboration], JHEP **1811**, 013 (2018) [arXiv:1802.09145].
- [64] The ATLAS collaboration, ATLAS-CONF-2017-012, <http://cds.cern.ch/record/2244824?ln=en>
- [65] V. Khachatryan *et al.* [CMS Collaboration], JHEP **1704**, 039 (2017) [arXiv:1611.01664].
- [66] S. Acharya *et al.* [ALICE Collaboration], Phys. Lett. **B788**, 166 (2019) [arXiv:1805.04399].

- [67] The ATLAS collaboration, ATLAS-CONF-2018-007, <http://cds.cern.ch/record/2318588>
- [68] A.M. Sirunyan *et al.* [CMS Collaboration], JHEP **1810**, 138 (2018) [arXiv:1809.00201].
- [69] R.J. Fries, B. Muller, C. Nonaka, and S.A. Bass, Phys. Rev. C**68**, 044902 (2003) [nucl-th/0306027].
- [70] V. Minissale, F. Scardina, and V. Greco, Phys. Rev. C**92**, 054904 (2015) [arXiv:1502.06213].
- [71] A. Adare *et al.* [PHENIX Collaboration], Phys. Rev. Lett. **105**, 142301 (2010) [arXiv:1006.3740].
- [72] B. Abelev *et al.* [ALICE Collaboration], Phys. Lett. B**719**, 18 (2013) [arXiv:1205.5761].
- [73] G. Aad *et al.* [ATLAS Collaboration], Phys. Lett. B**707**, 330 (2012) [arXiv:1108.6018].
- [74] S. Chatrchyan *et al.* [CMS Collaboration], Phys. Rev. Lett. **109**, 022301 (2012) [arXiv:1204.1850].
- [75] M. Aaboud *et al.* [ATLAS Collaboration], Eur. Phys. J. C**78**, 997 (2018) [arXiv:1808.03951].
- [76] A.M. Sirunyan *et al.* [CMS Collaboration], Phys. Lett. B**776**, 195 (2018) [arXiv:1702.00630].
- [77] S. Acharya *et al.* [ALICE Collaboration], Phys. Lett. B**784**, 82 (2018) [arXiv:1805.01832].
- [78] G. Aad *et al.* [ATLAS Collaboration], Phys. Rev. C**101**, 024906 (2020) [arXiv:1911.04812].
- [79] A.M. Sirunyan *et al.* [CMS Collaboration], Phys. Rev. C**100**, 044902 (2019) [arXiv:1901.07997].
- [80] K.M. Burke *et al.* [JET Collaboration] Phys. Rev. C**90**, 014909 (2014) [arXiv:1312.5003].
- [81] X. Feal, C.A. Salgado, and R.A. Vazquez, [arXiv:1911.01309].
- [82] J. Liao and E. Shuryak, Phys. Rev. C**75**, 054907 (2007) [arXiv:hep-ph/0611131].
- [83] J. Xu, J. Liao, and M. Gyulassy, Chin. Phys. Lett. **32**, 092501 (2015) [arXiv:1411.3673].
- [84] B.G. Zakharov, JETP Lett. **101**, 587 (2015) [arXiv:1412.6287].
- [85] B.G. Zakharov, J. Phys. G**41**, 075008 (2014) [arXiv:1311.1159].
- [86] B.G. Zakharov, Phys. Rev. Lett. **112**, 032301 (2014) [arXiv:1307.3674].
- [87] J.-Y. Ollitrault, Eur. J. Phys. **29**, 275 (2008) [arXiv:0708.2433].
- [88] A. Kisiel, W. Broniowski, M. Chojnacki, and W. Florkowski, Phys.Rev. C**79**, 014902 (2009) [arXiv:0808.3363].
- [89] R. Baier, A.H. Mueller, and D. Schiff, Phys. Lett. B**649**, 147 (2007) [nucl-th/0612068].
- [90] T. Renk, J. Ruppert, C. Nonaka, and S.A. Bass, Phys. Rev. C**75**, 031902 (2007) [nucl-th/0611027].
- [91] N.N. Nikolaev and B.G. Zakharov, Z. Phys. C**64**, 631 (1994) [arXiv:hep-ph/9306230].
- [92] R. Baier, Y.L. Dokshitzer, A.H. Mueller, and D. Schiff, JHEP **0109**, 033 (2001) [arXiv:hep-ph/0106347].
- [93] M. Gyulassy, P. Levai, and I. Vitev, Phys. Lett. B**538**, 282 (2002) [arXiv:nucl-th/0112071].
- [94] B.G. Zakharov, JETP, **125**, 1071 (2017) [arXiv:1706.03980].